Radial distribution of wood extractives in European larch Larix decidua by TOF-SIMS imaging

Tingting Fu, Nicolas Elie, Alain Brunelle

Radial distribution of wood extractives in European larch *Larix decidua* by TOF-SIMS imaging

Tingting Fu, Nicolas Elie, and Alain Brunelle*

Institut de Chimie des Substances Naturelles, CNRS UPR 2301, Univ. Paris-Sud, Université Paris-Saclay, Gif-sur-Yvette, France.

Abstract

Wood extractives in the xylem of European larch *Larix decidua* were mapped by time-of-flight secondary ion mass spectrometry (TOF-SIMS) imaging, which allows the radial distribution of both mineral and lipophilic extractives in the xylem to be scrutinized with high spatial resolution for the first time. Results show that all the components are inhomogeneously distributed across the annual ring. Mineral nutrients including Na^+, K^+, Ca^+, and Cl^- ions exhibit no preferential localization between earlywood and latewood, whereas PO_3^- ion is exclusively present in the ray cells, indicating it may be related to acid phosphatase. Lipophilic extractives were found to be more abundant in the inner secondary xylem. Ion images with 400 nm spatial resolution reveal that fatty acids, triglycerides and phytosterols are co-localized principally in the earlywood within the first annual ring. Resin acids prove to be the main components in the resin canal of the secondary xylem and are distributed in the outer of it.

Highlights

- Mass spectrometry imaging of wood extractives in European larch *Larix decidua*.
- Measurement of the radial distribution of mineral and organic compounds.
- Inhomogeneous distribution of the components across the annual ring.

Keywords

Mass Spectrometry imaging, TOF-SIMS, European larch, mineral nutrients, phosphate, triglycerides, phytosterols, resin acids.

Corresponding author

E-mail address: Alain.Brunelle@cnrs.fr (Alain Brunelle)

1. Introduction

Wood extractives are solvent extractable components in wood tissues, comprising of a variety of compounds such as fatty acids, sterols, phenols, and so on (Rowell, 2005). These extractives play an important role in decay resistance to termite, fungi, and environmental stress.

European larch (Pinaceae *Larix decidua* Mill.) is an important conifer species endemic to alpine forests in western and central Europe. In France, it is found mainly in Briançonnais, Queyras, Ubaye, Dévoluy, and Mercantour. The fast-growing nature and good durability make it a valuable timber tree of which the wood is widely used in carpentry, especially in making waterproof objects that can be used outdoors (Da Ronch, 2016). For example, traditional roofs in Briançonnais are made of larch shingles. It has been revealed that, as a property shared by many hardwood and softwood trees, the natural durability of larch wood is due to its decay resistance to microbial deterioration. The quantity and composition of heartwood extractives vary dramatically among different larch species, and there is a close correlation between extractive contents and natural durability (Windeisen, 2002; Gierlinger, 2004a). In addition, heartwood extractives could also affect the wood quality including mechanical property (Grabner, 2005) and stability (Panday, 2005; Shebani, 2008).

Conventionally, the extractives were roughly classified into organic solvent extractives, water extractives, and phenolics, which were then determined by solvent extraction or more rapidly by Fourier transform near infrared (FTNIR) spectroscopy (Gierlinger, 2002). Nevertheless, precise characterization of the chemical composition of some larch species has also been performed with gas chromatography (GC) (Zule, 2015) and liquid chromatography (LC) (Ostroukhova, 2012)-mass spectrometry (MS). However, very few studies concerning the spatial distribution of the extractives have been carried out. Spatial distribution of the extractives is very important in understanding heartwood formation and it largely determines the wood quality (Taylor, 2002). Radial distribution of European larch extractives has been examined by Gierlinger *et al.* (Gierlinger, 2004b) through micro-sampling of wood blocks which were subsequently analyzed by FTIR. Their results have shown that in mature larch the amount of the wood extractives increase linearly from pith to the heartwood/sapwood boundary. Similar sampling method followed by GC analyses was also applied to scrutinize the chemical compositional difference in earlywood and latewood of spruce (Bertaud, 2004) and radial distribution of extractives in scots pine wood (Ekeberg, 2006). However, this manual sampling method leads to limited spatial resolution and could not provide cellular localization of the extractives. The time consuming extraction with toxic solvents has also to be considered.

Time-of-flight secondary ion mass spectrometry (TOF-SIMS) is a surface analytical technique, which is recognized by its high spatial resolution. By dividing a certain analytical area into pixels and recording mass spectra from each pixel, TOF-SIMS provides simultaneously chemical and spatial information of the sample surface. Although traditionally employed for analysis of inorganic materials, TOF-SIMS has been gaining its reputation in biological imaging since the development of cluster ion beams (for example, Bi_3^+, Au_3^+, C_{60}^+) which has effectively improved the capability of providing direct molecular information up to *m/z* 1500 (Winograd, 2005; Brunelle, 2005; Bich, 2014). Concurrently, the number of studies using TOF-SIMS to map chemical constituents in wood tissues is also increasing. In addition to inorganic ions (Tokareva, 2007) and fragments of wood structural polymer lignin and polysaccharides (Saito, 2012; Jung, 2012), specific extractives such as diterpene phenol (Imai, 2005), hinokinin and its derivatives (Saito, 2008), and tryptamine (Vanbellingen, 2016) in various wood species have been mapped by TOF-SIMS.

In this study, TOF-SIMS was employed to investigate the spatial distribution of extractives in the branch wood of European larch (*Larix decidua* Mill.). Large area analysis of the xylem wood was performed to examine the radial distribution of wood extractives from the pith towards the secondary xylem. Meanwhile, cellular localization of the extractives in earlywood and latewood within different annual rings was revealed with a high spatial resolution of 400 nm. Different localization patterns were observed for mineral ions and organic extractives, whereas the extractive species are heterogeneously distributed in the secondary xylem.

2. Results and discussion

2.1. Large area imaging and distribution of mineral nutrients

To examine the radial distribution of wood extractives from pith towards the secondary xylem in the larch branch, a large area of 3000 µm × 500 µm was first mapped by TOF-SIMS. Although wood extractives generally refer to extractable organic components, mineral elements also constitute an important part of the extractives and different translocation patterns of mineral elements have been observed in heartwood formation (Taylor, 2002). Therefore, the mineral ions in the branch heartwood were also investigated in addition to the organic constituents. Figure 1 illustrates the distributions of mineral ions in the xylem as well as in the pith. It is found that very little Cl^- and Na^+ are present in the xylem. Also interesting to note is that Cl^- is well co-localized with Na^+, indicating that Cl^- is mainly associated with Na^+ in larch wood, although K^+ turns out to be more abundant than Na^+ in the larch branch. Calcium shows similar distribution to K^+, however with lower intensity. Calcium has low mobility in plant tissues and plays an important role in physiological process and environmental response (McLaughlin, 1999). Phosphate was exclusively detected in the ray cells and is probably related

to acid phosphatase, which is believed to facilitate the transport of carbohydrates in wood tissues through the phosphorylation/dephosphorylation process (Sauter, 1972). The ion images demonstrate that except from the ray cell-specific phosphate, all the other minerals show heterogeneous distribution in the secondary xylem and no obvious preferential distribution between earlywood and latewood. In all the cases, minimum amount of mineral nutrients is present in the pith and primary xylem. Besides endogenous mechanisms (Chun, 1992), variations in the concentration of the minerals across the annual rings may also reflect the environmental influence (Penninckx, 2001).

2.2. Radial distribution of lipophilic extractives

Organic extractives are more abundant than inorganic minerals in wood. They constitute an important proportion of wood chemistry and comprise a wide range of non-structural lipophilic compounds. To scrutinize the precise localization of the organic components, three different regions presenting wood tissue within different annual rings in the xylem were mapped with high spatial resolution of 400 nm (Figure 2a). Figure 2b shows TOF-SIMS mass spectra obtained from the three different analyzed areas in both positive and negative polarities. Similar to the inhomogeneous distribution of mineral nutrients, the comparison of spectra from the three different regions indicates the relative abundance of the organic extractive also varies dramatically throughout the xylem. The composition and radial distribution of fatty acids, glycerides, resin acids, and phytosterols will be discussed in detail in the following paragraphs. Table 1 summarizes the chemical species which are detected in the positive and negative ion mass spectra, with their measured and calculated mass-to-charge ratio, mass deviation in ppm, assignments and literature references. Assignments of fatty acids, diglycerides, and triglycerides were made according to the literature (Tokareva, 2007; Debois, 2008; Debois, 2009), and especially thanks to a study made by our lab of human liver steatosis (Debois, 2008; Debois, 2009). In addition, the ethyl acetate extract from the Larch sample was analyzed by LC-MS, helping the assignments of the fatty acid ion species. The corresponding chromatogram and extracted mass spectra are shown in Figures S1 to S7. Assignments of ions from resin acid and phytosterols were made according to the TOF-SIMS analyses of pure standards of abietic acid,campesterol, stigmasterol, and β-sitosterol. We did not analyze pure brassicasterol and cycloartenol, because the purchase of these was too expensive, even in very small quantities. The corresponding TOF-SIMS mass spectra are shown in Figures S8 and S9, respectively. The ion peaks at *m/z* 502.3 in the positive mass spectrum and *m/z* 501.4 in the negative spectrum were unable to be identified. In addition, the most abundant phenol compound taxifolin in the knotwood of *Larix decidua* (Kebbi-Benkeder, 2015) was not detected here, probably due to compositional variation in different anatomic plant parts.

2.3. Glycerides and fatty acids

Glycerides and fatty acids are common extractives present in various wood species. As shown in Figure 2b, ion peaks corresponding to fatty acids were detected in the negative mass spectra: *m/z* 255.2 ($C_{16}H_{31}O_2^-$, palmitic acid), *m/z* 269.2 ($C_{17}H_{33}O_2^-$, heptadecanoic acid), *m/z* 277.2 ($C_{18}H_{29}O_2^-$, α-linoleic acid), *m/z* 279.2 ($C_{18}H_{31}O_2^-$, linoleic acid), and *m/z* 281.2 ($C_{18}H_{33}O_2^-$, oleic acid). Meanwhile, triglycerides were mainly detected as diglycerides fragments $[M-H_2O+H]^+$ in the positive mass spectra (Tokareva, 2007): *m/z* 573.5 ($C_{37}H_{65}O_4^+$, DG34:3), *m/z* 575.5 ($C_{37}H_{67}O_4^+$, DG34:2), *m/z* 577.5 ($C_{37}H_{69}O_4^+$, DG34:1), *m/z* 595.5 ($C_{39}H_{63}O_4^+$, DG36:6), *m/z* 597.5 ($C_{39}H_{65}O_4^+$, DG36:5), *m/z* 599.5 ($C_{39}H_{67}O_4^+$, DG36:4), *m/z* 601.5 ($C_{39}H_{69}O_4^+$, DG36:3), *m/z* 603.5 ($C_{39}H_{71}O_4^+$, DG36:2). Mass assignments of these fatty acid and diglyceride ion species were made thanks to previous analyses of lipids in human liver (Debois, 2008; Debois, 2009). Figure 3 displays the radial distribution of fatty acids and triglycerides in the xylem (the positive and negative total ion images are shown in Figure S10). Ion images of fatty acids and triglycerides were summed up, respectively, revealing that they have identical localization mainly in the earlywood within the first annual ring around the pith (Figure 3a and 3b). Triglycerides make up the main composition of fats in wood and serve as energy source for the cells. However, hydrolysis of triglycerides will occur when secondary xylem is formed, which partly explains their low abundance apart from the low ionization/desorption efficiency and fragmentation during SIMS analysis. High resolution images further show the accumulation of fatty acids and triglycerides in the inner earlywood and their diffusion into the surrounding cells (Figure 3c-3h). Nevertheless, fatty acids and triglycerides are also present in the resin canal in a noticeable amount.

2.4. Resin acids

Apart from phenolic compounds, resin acids also contribute significantly to protecting the wood from insects and microbial deterioration (Harju, 2002). Comparing the high resolution mass spectra recorded in the three regions leads to the differentiation of the specific presence of the negative ion at *m/z* 301.2 in region 3 (Figure 2b). Reconstruction of the ion image in Figure 4 reveals that this compound is almost exclusively located in the resin canal. Therefore, the ion at *m/z* 301.2 is attributed to resin acid ($C_{20}H_{30}O_2$, MW 302.2, Table 1, Figure S8) which is probably a mixture of abietic-type acids and pimaric-type acids since they are both predominantly present in European larch (Zule, 2015; Ostroukhova, 2012). Noticeably, abietic acid and isopimaric acid (Figure 4), which represent the two types of resin acids, respectively, are the most abundant resin acids in larch. The three-color overlay of ion images from resin acids (blue), fatty acids (green) and total ions (red) directly illustrates the distinct localizations of these two lipophilic extractives (Figure 4c). Chemical composition of the resin canal was further examined by manually selecting a region of interest of this specific structure. The

corresponding negative ion mass spectrum is illustrated in Figure 4d, showing that apart from a minimum amount of fatty acids, resin acid is the main component of the resin canal.

2.5. Phytosterols

Phytosterols are plant sterols, which are essential components of plant cell membrane in the same way as cholesterol in mammalian cells (Piironen, 2000). Figure 5 shows a partial positive mass spectrum with the peaks of the main phytosterols detected in TOF-SIMS. In accordance with a previous study (Zule, 2015), *β*-sitosterol is found to be the most abundant in the larch xylem and was detected as dehydrated fragment ion at *m/z* 397.4 ($C_{29}H_{49}^+$) (Tokareva, 2007). An ion with the same mass-to-charge ratio was detected from a solution of pure *β*-sitosterol (Figure S9, Table 1) Some neighbor ion peaks at 383.4 ($C_{28}H_{47}^+$), and 395.4 ($C_{29}H_{47}^+$)can be assigned to campesterol, and stigmasterol, respectively. This is supported by the analyses of the pure standards, of which the mass spectra are shown in Figure S9 (Table 1). Ions peaks at *m/z* 381.4 and 409.4 are likely to be also characteristic of other phytosterol species, and can be attributed to brassicasterol ($C_{28}H_{45}^+$) and cycloartenol ($C_{30}H_{49}^+$), respectively, although not confirmed by another analysis. The radial distribution of phytosterols is illustrated in Figure 6. The large area chemical map (Figure 6a) shows that phytosterols concentrate in the earlywood within the first annual ring and they are rarely present in the outer secondary xylem. High-resolution ion images (Figure 6b-6d) reveal that phytosterols are well co-localized with fatty acids and triglycerides in the inner earlywood in all the three analyzed regions. In addition, the ion images demonstrate that the inner secondary xylem comprises a higher amount of lipophilic extractives (fatty acids, glycerides, and phytosterols) than the outer secondary xylem. Detailed radial distribution of wood extractives within a few annual rings in larch has not been investigated before. These results reveal that their distribution patterns are similar to other softwood species such as Norway spruce (Bertaud, 2004) and Scots pine (Ekeberg, 2006).

3. Conclusion

TOF-SIMS imaging was applied to reveal the chemical composition, and the radial distribution of it, in the xylem of European larch *Larix decidua*. The *in situ* characterization of the extractives by TOF-SIMS proves to be a precise and rapid analytical method for examination of the radial distribution of wood extractives. High resolution mapping of both inorganic and organic extractives establishes the inhomogeneous distribution of the chemical contents. Mineral nutrients exhibit no preferential localization except phosphate which is probably involved in the phosphorylation/dephosphorylation process to facilitate the transport of carbohydrates in wood. Lipophilic extractives including fatty acids, glycerides and phytosterols were found to be more abundant in the inner secondary xylem, whereas resin acids were mostly found in the outer secondary xylem due to their specific localization in the resin canal. In

contrary to inorganic compounds, all the lipophilic compounds are revealed to be mainly localized in the earlywood . The results indicate that in addition to the main chemical constituents, the distribution pattern is also similar to other conifer genera such as pine and spruce. Lipophilic extractives are essential metabolites responsible for the endogenous metabolism and natural decay resistance of the wood. Thus scrutiny of radial distribution of the extractives will contribute to a better understanding of heartwood formation and wood quality control.

4. Experimental

4.1. Analysis of standards

Pure standards of abietic acid, campesterol (Sigma-Aldrich, Saint-Quentin Fallavier, France), stigmasterol, and β-sitosterol (CNRS-ICSN extractothèque, 2018) were prepared at a concentration of 1 mg/mL in CH_2Cl_2. 1 µL of each solution was deposited on a silicon wafer in order to record reference TOF-SIMS positive and negative ion mass spectra. Analyses were performed with a primary ion dose of 1.0×10^{11} ions/cm^2.

4.2. Plant material

Larch samples are from the upper part of the Vallouise valley, in the small valley of torrent de Saint-Pierre, in France (area of Pelvoux village, exact GPS coordinates 6°26’31’’ E and 44°53’49’’ N) (Google Maps/Google Earth, 2018), at an altitude of 1572 m. The branch wood was collected from a several-year-old larch tree in the August of 2015, and was kept under ambient environment afterwards. Previous reports have shown that the branch heartwood contains relatively more extractives than the stem wood (Morikawa, 2012; Wen-jie, 2005). The sample used in the present study was not originating from a trunk but only from a small branch, which was a few years old. Since there is strong correlation between the age of cambium and heartwood formation (Nawrot, 2008), we are not certain about the presence of heartwood

4.3. Wood surface preparation

Before analysis, the bark was removed and the remaining stem was trimmed with a razor blade to generate a small block of about 1 cm × 1 cm × 1 cm. A transverse surface of approximately 1 mm × 3 mm was obtained with ultramicrotome (EM UC6, Leica Microsystèmes, SAS, Nanterre, France) using a diamond knife (DIATOME Cryotrim 45°, Leica Microsystèmes, SAS, Nanterre, France). The cutting was performed at a speed of 2 mm/s with a fixed cutting feed of 200 nm. The clearance angle was kept constant at 6° during the sectioning. Optical images of wood surfaces were acquired at ×10 magnification with an Olympus BX51 microscope (Rungis, France) equipped with a motorized scanning stage (Marzhauser Wetzlar GmbH, Wetzlar, Germany), a SC30 color camera, and monitored by the Olympus Stream

Motion 1.9 software. Extended focal imaging (EFI) scanning mode was applied to improve the image quality.

4.4. TOF-SIMS imaging analysis

Mass spectrometry imaging experiments were performed with a commercial TOF-SIMS IV (ION-TOF GmbH, Münster, Germany) mass spectrometer equipped with a bismuth liquid metal ion gun (LMIG). Mass spectra and ion density images were acquired using Bi_3^+ cluster ions as primary ion beam with a kinetic energy of 25 keV. Large area imaging was carried out with the so-called high current bunched ion focusing mode where the current measured at 10 kHz was 0.38 pA. The imaged area was 3000 µm × 500 µm divided by 768 pixels × 128 pixels, resulting in a spatial resolution of about 4 µm. The ion dose density applied was 1.25×10^{10} ions/cm^2. High resolution images were recorded with burst alignment ion focusing mode to obtain a high lateral resolution of 400 nm. In this case, the primary ion pulse duration was set at 100 ns and the current measured at 10 kHz was 0.074 pA. An extraction delay of the secondary ions was employed to improve mass resolution (Vanbellingen, 2015). The attainable mass resolution was ~ 6 000 at *m/z* 279.2 ($C_{18}H_{31}O_2^-$). Three individual areas of 400 µm × 400 µm were imaged with 1024 × 1024 pixels and an ion dose density of 3×10^{12} ions/cm^2. A low energy pulsed electron flood gun (21 eV) was applied to neutralize the charges accumulated on the insulating surface. Data processing was performed using SurfaceLab 6.7 (ION-TOF GmbH, Münster, Germany), and the primary ion beam shift during the acquisitions was corrected by 'lateral shift correction' function in the software. Mass spectra were calibrated using lignin and polysaccharides fragment ions (Goacher, 2011) such as $C_7H_7^+$, $C_7H_9^+$, $C_7H_{11}^+$, $C_8H_7^+$, $C_8H_{11}^+$, $C_9H_{11}^+$, $C_{10}H_{11}^+$, $C_{11}H_9O_3^+$ in positive ion mode and light fragments C_4H^-, $C_4H_3^-$, $C_3H_3O^-$, $C_3H_5O^-$, $C_3H_3O_2^-$ in negative ion mode. No normalization of the ion images was performed, either with respect to a particular ion, or with respect to the total ion image. Ion images were all recorded with the same primary ion dose, so are directly comparable to each other. The only limitation is that matrix effects may always exist, causing the ionic emission of a particular ion to increase or decrease because of its microenvironment. This does not preclude, however, the relative comparison of the emission of a particular ion between histologically comparable zones.

In the secondary ion images, the name of the compound or the *m/z* value of the corresponding ion, the maximum counts in a pixel (MC) and the total counts (TC) are shown below each image (except for color overlays). The color scales correspond to the interval [0, MC].

4.5. Solvent extraction and LC-MS analysis of larch wood

Larch sample from the same branch wood was ground into small pieces and particles before being extracted with ethyl acetate using an accelerated solvent extractor (ASE300, DIONEX).

The extraction was carried out with three cycles. For each cycle, the wood sample was heated to 40 °C for 5 min and then extracted for another 5 min under a pressure of 100 bar. After the extraction, ethyl acetate was removed using a rotary evaporator and the dried extract was stored at -20 °C before analysis.

LC-MS analysis was performed on a HPLC Ultimate 3000 system (Dionex, Voisins-le-Bretonneux, France) coupled with an Agilent 6540 Q-ToF (Agilent Technologies, Waldbronn, Germany) mass spectrometer. Electrospray ion source was utilized for the analysis. The larch wood extract was injected at 1.0 mg/mL in methanol and the separation was carried out in an Accucore RP-MS column (100 × 2.1 mm, 2.6 µm, Thermo Scientific, Courtaboeuf, France) with a mobile phase consisting of water (A) and acetonitrile (B) (both A and B contain 0.1 % formic acid). Compounds were eluted at a flow rate of 0.4 mL/min with a gradient from 5 % B to 100 % B in 25 min and then 100 % B for 3 min. Mass spectra were recorded with the following parameters: spray voltage set at 3.5 kV, capillary temperature at 325 °C, capillary voltage at 45 V and fragmentor voltage at 140 V. Internal calibration was achieved with two calibrants (*m/z* 121.0509 and *m/z* 922.0098) providing a high mass accuracy of better than 5 ppm. Mass resolution was 20,000 at *m/z* 922.0098.

Acknowledgements

This work has benefited from an ‘Investissement d’Avenir’ grant managed by Agence Nationale de la Recherche (CEBA, ref. ANR-10-LABX-25-01) and was financially supported by the Agence Nationale de la Recherche (France, grant ANR-2015-CE29-0007-01 DEFIMAGE). TF would like to acknowledge financial support from China Scholarship Council (CSC, No. 201406310013). This work has benefited from the facilities and expertise of the Electron Microscopy facilities of Imagerie-Gif (http://www.i2bc.paris-saclay.fr/spip.php?article282). Fruitful discussions with Stéphane Dumarcay (INRA, Nancy, France) were greatly appreciated.

Associated content

Supporting Information
Supplementary figures S1-S10.

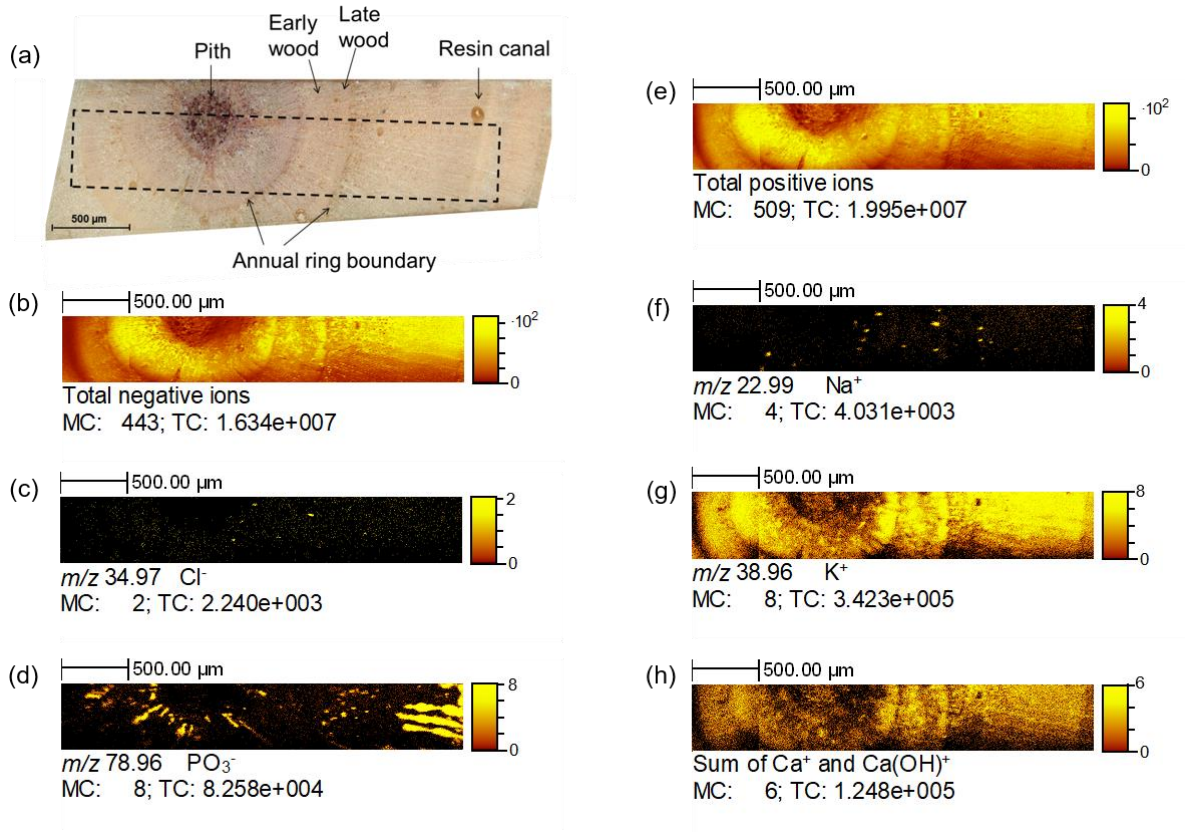

Figure 1:

Radial distribution of mineral ions in the branch xylem of *Larix decidua*. (a) Microscopic image of the transverse surface of the branch xylem. The black dotted rectangle indicates the area imaged by TOF-SIMS. (b) Total negative ion image. (c) Ion image of Cl^-. (d) Ion image of PO_3^-. (e) Total positive ion image. (f) Ion image of Na^+. (g) Ion image of K^+. (h) Ion image of the sum of Ca^+ and $Ca(OH)^+$.

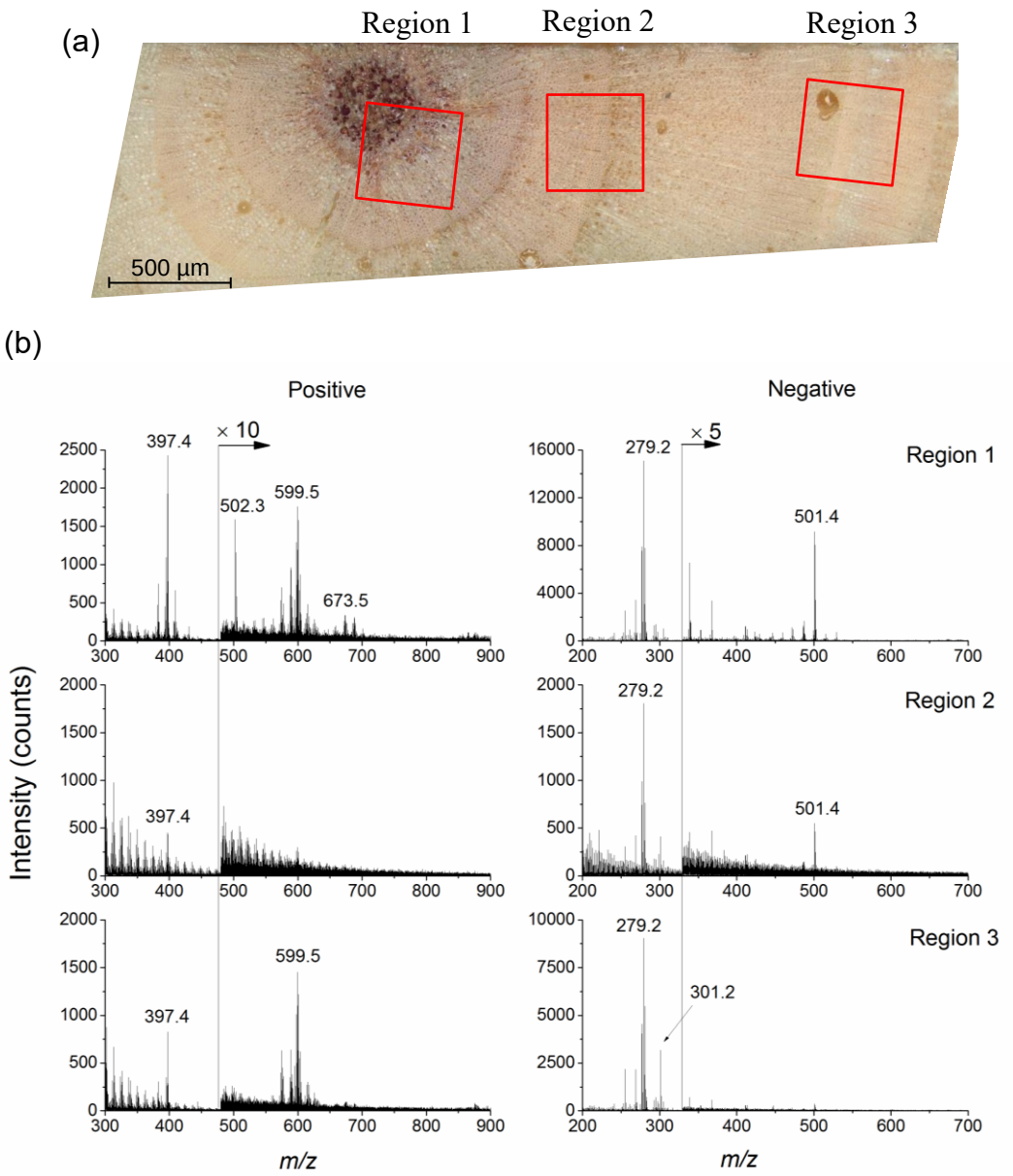

Figure 2: TOF-SIMS analysis of the branch xylem of *Larix decidua*. (a) Optical image. The red squares indicate the three regions analyzed with 400 nm resolution. Region 1: pith to secondary xylem; Region 2, second annual ring with both earlywood and latewood ; Region 3: third annual ring with both earlywood and latewood ; (b) Partial TOF-SIMS mass spectra (left column: positive ion mass spectra; right column: negative ion mass spectra) showing organic composition in the three regions.

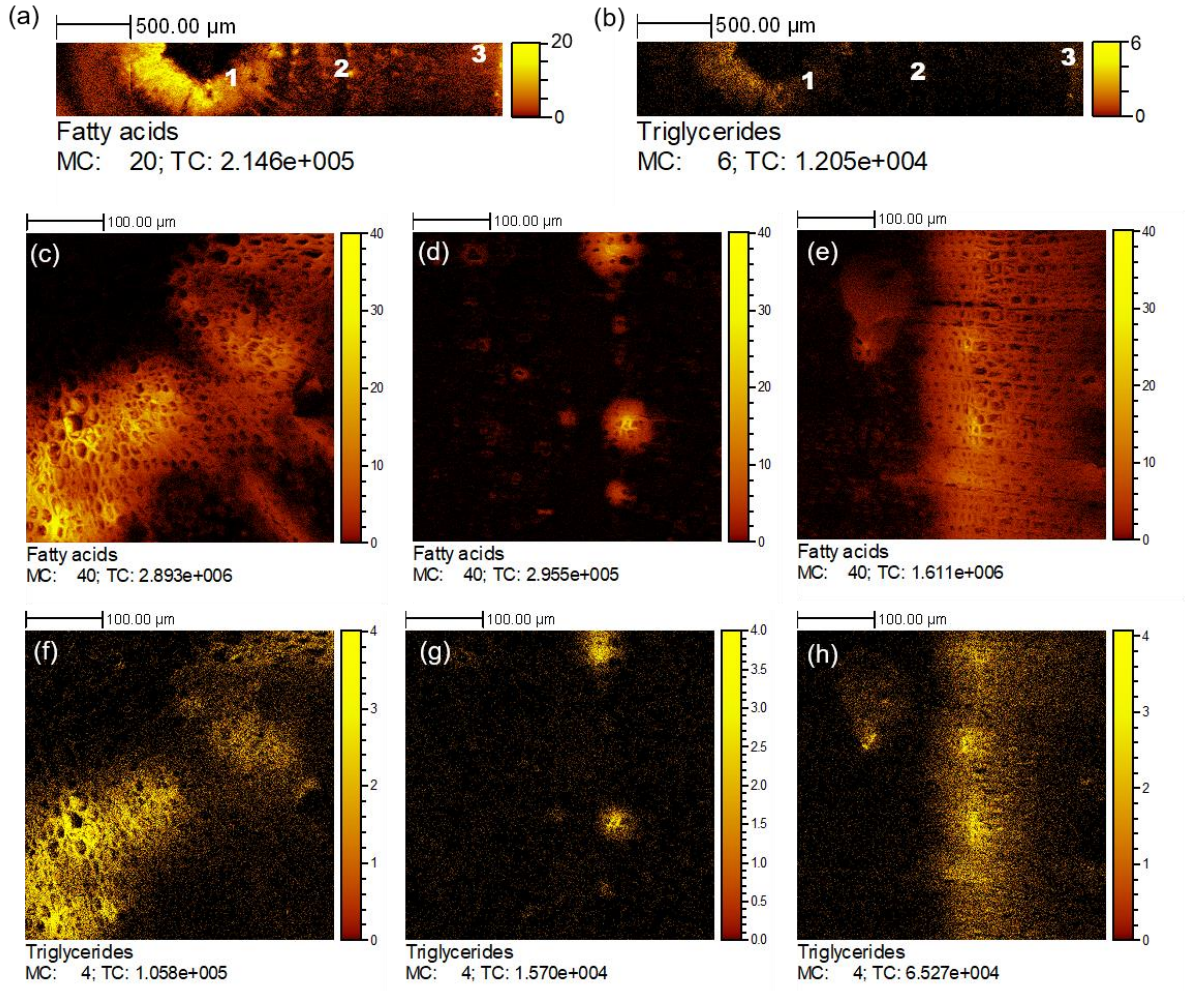

Figure 3: Radial distribution of fatty acids and triglycerides in branch xylem of *Larix decidua*. (a) Summed negative ion images of fatty acids from large area analysis; (b) Summed positive ion images of triglycerides from large area analysis; (c) to (e): High resolution localization of negative ions of fatty acids in region 1 (c), region 2 (d), and region 3 (e). (f) to (h): High resolution localization of positive ions of triglycerides in region 1 (f), region 2 (g) and region 3 (h). The triglyceride ion images in f, g, and h are binned to 4 pixels to enhance the visibility. The three regions are indicated in Figure 2a.

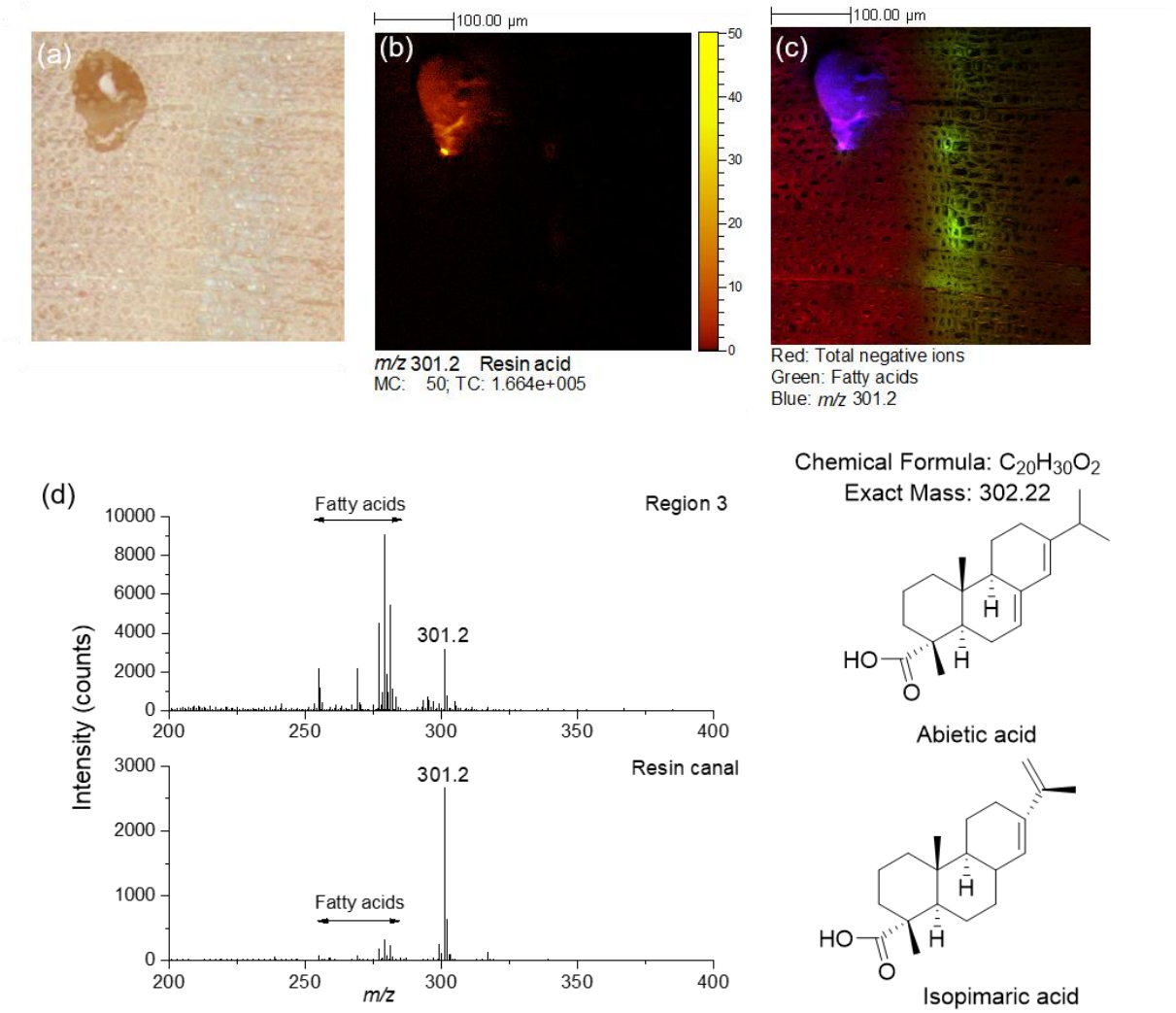

Figure 4: Localization of resin acids in the resin canal. (a) Optical image of region 3 with a resin canal; (b) High resolution negative ion image of resin acids in region 3; (c) Three color overlay between three different negative ions: total negative ions (red), fatty acids (green), and resin acid (blue) (*m/z* 301.2); (d) TOF-SIMS negative ion mass spectra of the whole region 3 (top) and region of interest (ROI) of the resin canal (bottom). Structures of abietic and pimaric acids are shown.

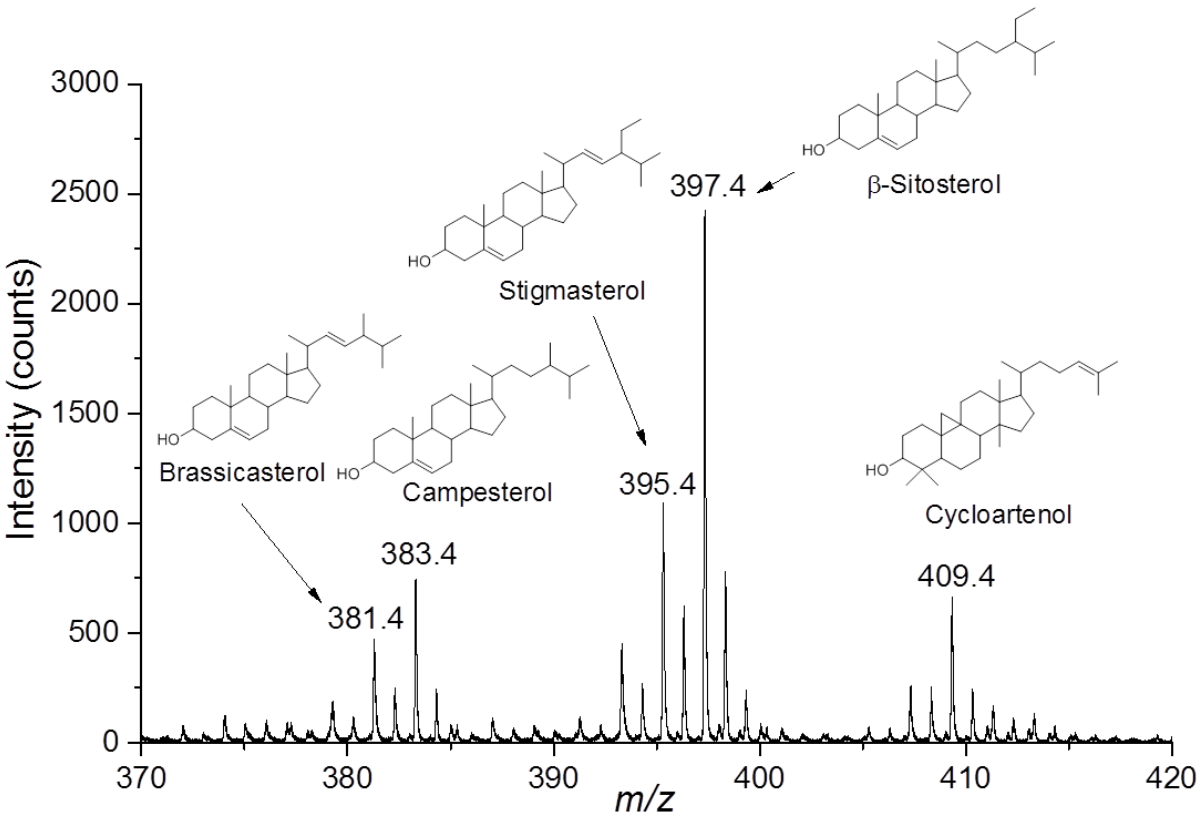

Figure 5: Partial positive TOF-SIMS spectrum obtained from region 1 showing the ion peaks corresponding to phytosterols, with chemical structures indicated above.

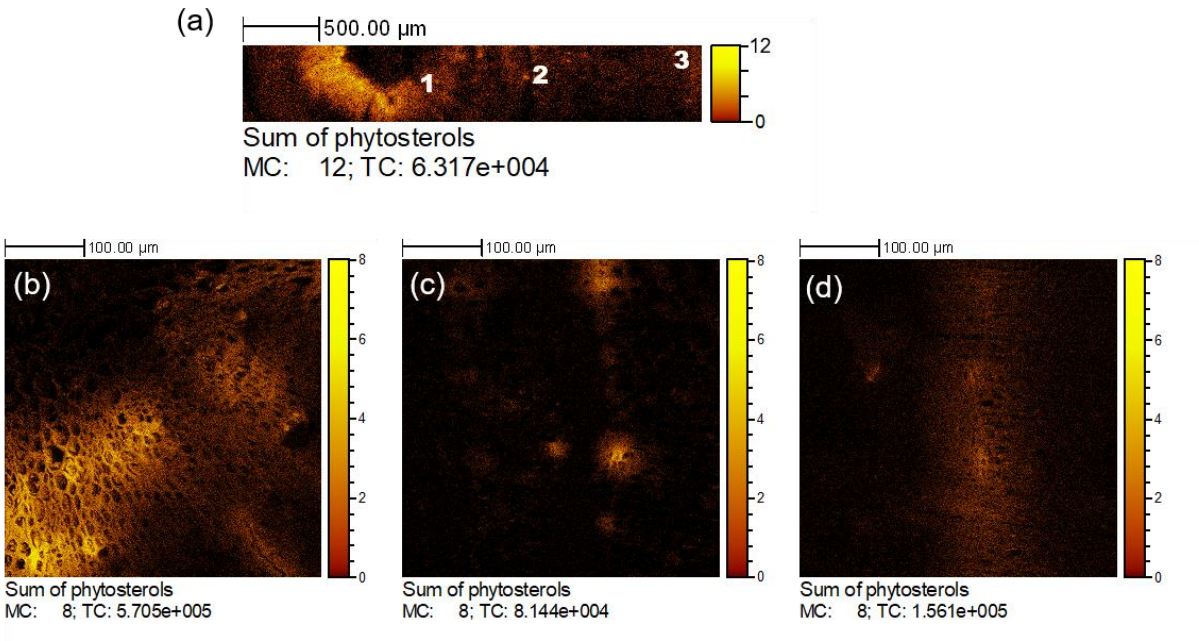

Figure 6: Radial distribution of phytosterol positive ions. (a) Summed ion images of phytosterols from large area analysis; (b) to (d): high resolution localization of phytosterols in region 1 (b), region 2 (c), and region 3 (d).

Table 1: Larch wood extractives detected in positive and negative ion modes.

Chemical species	Polarity	Measured mass (m/z)	Theoretical mass (m/z)	Mass deviation (ppm)	Assignment
Phytosterol $[M-H_2O+H]^+$	+	381.36	381.35	26	$C_{28}H_{45}^+$, brassicasterol
		383.36	383.37	-26	$C_{28}H_{47}^+$, Campesterol
		395.36	395.37	-25	$C_{29}H_{47}^+$, Stigmasterol
		397.38	397.38	-18	$C_{29}H_{49}^+$, β-Sitosterol (Tokareva, 2007)
		409.38	409.38	-15	$C_{30}H_{49}^+$, Cycloartenol
Diglyceride $[M-H_2O+H]^+$	+	573.47	573.49	-35	$C_{37}H_{65}O_4^+$, DG34:3 *
		575.49	575.50	-17	$C_{37}H_{67}O_4^+$, DG34:2 *
		577.50	577.52	-35	$C_{37}H_{69}O_4^+$, DG34:1 *
		595.47	595.47	3.0	$C_{39}H_{63}O_4^+$, DG36:6 *
		597.48	597.49	-17	$C_{39}H_{65}O_4^+$, DG36:5 *
		599.49	599.50	-17	$C_{39}H_{67}O_4^+$, DG36:4 *
		601.51	601.52	-17	$C_{39}H_{69}O_4^+$, DG36:3 *
		603.52	603.53	-17	$C_{39}H_{71}O_4^+$, DG36:2 *
Fatty acid $[M-H]^-$	-	255.22	255.23	-39	$C_{16}H_{31}O_2^-$, palmitic acid
		269.24	269.25	-37	$C_{17}H_{33}O_2^-$, heptadecanoic acid
		277.21	277.22	-36	$C_{18}H_{29}O_2^-$, α-linoleic acid
		279.22	279.23	-36	$C_{18}H_{31}O_2^-$, linoleic acid
		281.24	281.25	-36	$C_{18}H_{33}O_2^-$, oleic acid
Resin acid $[M-H]^-$	-	301.21	301.22	-33	$C_{20}H_{29}O_2^-$

* Assignments of diglyceride ions according to (Tokareva, 2007) and (Debois, 2008; Debois, 2009)

References

Bertaud, F., Holmbom, B., 2004. Chemical composition of earlywood and latewood in Norway spruce heartwood, sapwood and transition zone wood. Wood Sci. Technol. 38, 245–256.

Bich, C., Touboul, D., Brunelle, A., 2014. Cluster TOF-SIMS imaging as a tool for micrometric histology of lipids in tissue. Mass Spectrom. Rev. 33, 442–451.

Brunelle, A., Touboul, D., Laprévote, O., 2005. Biological tissue imaging with time-of-flight secondary ion mass spectrometry and cluster ion sources. J. Mass Spectrom. 40, 985–999.

Chun, L., Hui-yi, H., 1992. Tree-ring element analysis of Korean pine (*Pinus koraiensis* Sieb. Et Zucc.) and Mongolian oak (*Quercus mongolica* Fisch. ex Turcz.) from Changbai Mountain, northeast China. Trees 6, 103–108.

Da Ronch, F., Caudullo, G., Tinner, W., de Rigo, D., 2016. Larix decidua and other larches in Europe: distribution, habitat, usage and threats, in: San-Miguel-Ayanz, J., de Rigo, D., Caudullo, G., Houston Durrant, T., Mauri, A. (Eds.), European atlas of forest tree species. Publication Office of the European Union, Luxembourg, pp. 108−110.

Debois, D., Bralet, M. P., Le Naour, F., Brunelle, A., Laprévote, O., 2009. In Situ Lipidomic Analysis of Nonalcoholic Fatty Liver by Cluster TOF-SIMS Imaging. Anal. Chem. 81, 2823−2831.

Ekeberg, D., Flæte, P. O., Eikenes, M., Fongen, M., Naess-Andresen, C. F, 2006. Qualitative and quantitative determination of extractives in heartwood of Scots pine (*Pinus sylvestris* L.) by gas chromatography. J. Chromatogr. A 1109, 267−272.

Gierlinger, N., Schwanninger, M., Hinterstoisser, B., Wimmer, R. 2002. Rapid determination of heartwood extractives in *Larix* sp. by means of Fourier transform near infrared spectroscopy. J. Near Infrared Spec. 10, 203–214.

Gierlinger, N., Jacques, D., Schwanninger, M., Wimmer, R., Pâques, L. E., 2004. Heartwood extractives and lignin content of different larch species (Larix sp.) and relationships to brown-rot decay-resistance. Trees 18, 230–236.

Gierlinger, N., Wimmer, R., 2004. Radial distribution of heartwood extractives and lignin in mature European larch. Wood Fiber Sci. 36, 387–394.

Goacher, R. E., Jeremic, D., Master, E. R., 2011. Expanding the library of secondary ions that distinguish lignin and polysaccharides in time-of-flight secondary ion mass spectrometry analysis of wood. Anal. Chem. 83, 804–812.

Grabner, M., Müller, U., Gierlinger, N., Wimmer, R., 2005. Effects of heartwood extractives on mechanical properties of larch. IAWA J. 26, 211–220.

Harju, A. M., Kainulainen, P., Venäläinen, M., Tiitta, M.; Viitanen, H., 2002. Differences in resin acid concentration between brown-rot resistant and susceptible scots pine heartwood. Holzforschung 56, 479–486.

Imai, T., Tanabe, K., Kato, T., Fukushima, K., 2005. Localization of ferruginol, a diterpene phenol, in Cryptomeria japonica heartwood by time-of-flight secondary ion mass spectrometry. Planta 211, 549–556.

Jung, S., Foston, M., Kalluri, U. C., Tuskan, G. A., Ragauskas, A. J., 2012. 3D chemical image using TOF-SIMS revealing the biopolymer component spatial and lateral distributions in biomass. Angew. Chem. Int. Edit. 51, 12005–12008.

Kebbi-Benkeder, Z., Colin, F., Dumarçay, S., Gérardin, P. 2015. Quantification and characterization of knotwood extractives of 12 European softwood and hardwood species. Ann. For. Sci. 72, 277–284.

McLaughlin, S. B., Wimmer, R., 1999. Calcium physiology and terrestrial ecosystem processes. New Phytol. 142, 373–417.

Morikawa, T., Ashitani, T., Sekine, N., Kusumoto, N., Takahashi, K., 2012. Bioactivities of extracts from *Chamaecyparis obtusa* branch heartwood. J. Wood Sci. 58, 544−549.

Nawrot, M., Pazdrowski, W., Szymański, M., 2008. Dynamics of heartwood formation and axial and radialdistribution of sapwood and heartwood in stems of European larch (*Larix decidua* Mill.). J. For. Sci. 54, 409−417.

Ostroukhova, L. A., Raldugin, V. A., Babkin, V. A., Onuchina, N. A., Levchuk, A. A., 2012. Investigation of the chemical composition of larch wood resin. Russ. J. Bioorg. Chem. 38, 775–779.

Pandey, K. K., 2005. A note on the influence of extractives on the photo-discoloration and photo-degradation of wood. Polym. Degrad. Stabil. 87, 375−379.

Penninckx, V., Glineur, S., Gruber, W., Herbauts, J., Meerts, P., 2001. Radial variations in wood mineral element concentrations: a comparison of beech and pedunculate oak from the Belgian Ardennes. Ann. For. Sci. 58, 253–260.

Piironen, V., Lindsay, D. G., Miettinen, T. A., Toivo, J., Lampi, A.-M., 2000. Plant sterols: biosynthesis, biological function and their importance to human nutrition. J. Sci. Food Agr. 80, 939–966.

Rowell, R. M., Pettersen, R., Han, J. S., Rowell, J. S., Tshabalala, M., A. 2005. Cell wall chemistry, in: Rowell, R. M., (Ed.), Handbook of wood chemistry and wood composites. CRC press, Boca Raton, Florida, pp. 33-74.

Saito, K., Mitsutani, T., Imai, T., Matsushita, Y., Fukushima, K., 2008. Discriminating the indistinguishable sapwood from heartwood in discolored ancient wood by direct molecular mapping of specific extractives using time-of-flight secondary ion mass spectrometry. Anal. Chem. 80, 1552–1557.

Saito, K., Watanabe, Y., Shirakawa, M., Matsushita, Y., Imai, T., Koike, T., Sano, Y., Funada, R., Fukazawa, K., Fukushima, K., 2012. Direct mapping of morphological distribution of syringyl and guaiacyl lignin in the xylem of maple by time-of-flight secondary ion mass spectrometry. Plant J. 69, 542–552.

Sauter, J. J., 1972. Respiratory and phosphatase activities in contact cells of wood rays and their possible role in sugar secretion. Z. Pflanzenphysiol. 67, 135−145.

Shebani, A. N., van Reenen, A. J., Meincken, M., 2008. The effect of wood extractives on the thermal stability of different wood species. Thermochim. Acta. 471, 43–50.

Taylor, A. M., Gartner, B. L., Morrell, J. J., 2002. Heartwood formation and natural durability–A review. Wood Fiber Sc. 34,587–611.

Tokareva, E. N., Fardim, P., Pranovich, A. V., Fagerholm, H.-P., Daniel, G., Holmbom, B., 2007. Imaging of wood tissue by ToF-SIMS: Critical evaluation and development of sample preparation techniques. Appl. Sur. Sci. 253, 7569–7577.

Vanbellingen, Q. P., Elie, N., Eller, M. J., Della-Negra, S., Touboul, D., Brunelle, A., 2015. Time-of-flight secondary ion mass spectrometry imaging of biological samples with delayed extraction for high mass and high spatial resolutions. Rapid Commun. Mass Spectrom. 29, 1187–1195.

Vanbellingen, Q. P., Fu T., Bich, C., Amusant, N., Stien, D., Della-Negra, S., Touboul, D., Brunelle, A., 2016. Mapping *Dicorynia guianensis* Amsh. wood constituents by submicron resolution cluster-TOF-SIMS Imaging. J. Mass Spectrom. 51, 412–423.

Wen-jie, W., Xue-ying, L., Yuan-gang, Z., 2005. Dynamic feature of flavonoids content in different organs of larch (*Larix gmelinii*). J. For. Res. 16, 89−92.

Windeisen, E., Wegener, G., Lesnino, G., Schumacher, P., 2002. Investigation of the correlation between extractives content and natural durability in 20 cultivated larch trees. Holz Roh Werkst. 60, 373−374.

Winograd, N., 2005. The Magic of Cluster SIMS. Anal. Chem. 77, 142A–149A.

Zule, J., Čufar, K., Tišler, V., 2015. Lipophilic Extractives in Heartwood of European Larch (*Larix decidua* Mill.). Drvna Ind. 66, 305−313.

Web References

Imagerie moléculaire d'échantillons biologiquespar spectrométrie de masse ToF-SIMS, Delphine Debois, PhD dissertation, Université d'Évry-Val d'Essonne, 2008.
https://www.biblio.univ-evry.fr/theses/2008/2008EVRY0014.pdf (accessed 31 January 2018)

Google Maps, Google Earth, 2017.
https://www.google.fr/maps/place/44%C2%B053'49%22N+6%C2%B026'31%22E/@44.8965408,6.4231335,4855m/data=!3m1!1e3!4m5!3m4!1s0x0:0x0!8m2!3d44.8970556!4d6.4421389?hl=fr (accessed 31 January 2018)

CNRS-ICSN extractothèque, 2018.
http://www.icsn.cnrs-gif.fr/spip.php?article586 (31 January 2018)